SIAM J. CONTROL OPTIM.
Vol. 51, No. 2, pp. 1372–1394

A NEW OPTIMAL CONTROL APPROACH FOR THE RECONSTRUCTION OF EXTENDED INCLUSIONS*

HABIB AMMARI†, PIERRE GARAPON‡, FRANÇOIS JOUVE§, HYEONBAE KANG¶, MIKYOUNG LIM‖, AND SANGHYEON YU‖

Abstract. The aim of this paper is to propose a new regularized optimal control formulation for recovering an extended inclusion from boundary measurements. Our approach provides an optimal representation of the shape of the inclusion. It guarantees local Lipschitz stability for the reconstruction problem. Some numerical experiments are performed to demonstrate the validity and the limitations of the proposed reconstruction method.

Key words. extended inclusion, reconstruction algorithm, optimal control, Helmholtz equation, shape representation, MUSIC algorithm, regularization

AMS subject classifications. 31B20, 35B37, 35L05

DOI. 10.1137/100808952

1. Introduction and problem formulation.

Let $\Omega \subset \mathbb{R}^d, d = 2, 3$, be a $\mathcal{C}^2$-bounded simply connected domain. Let ν denote the outward normal to the boundary $\partial\Omega$. Suppose that Ω contains an inclusion D_* of class $\mathcal{C}^{2,\eta}$ $(0 < \eta < 1)$, away from the boundary, with a known material parameter, such as the conductivity, $0 < k \neq 1 < +\infty$. We assume the material parameter of the background to be 1. Throughout this paper γ_{D_*} denotes the material parameter distribution, namely,

$$\gamma_{D_*} = 1 + (k-1)\chi[D_*], \tag{1.1}$$

where χ is the characteristic function.

For $l = 1, \ldots, N$, we denote by $u_*^{(l)}$ the solution to the following Helmholtz equation:

$$\begin{cases} \nabla \cdot \gamma_{D_*} \nabla u_*^{(l)} + \omega^2 u_*^{(l)} = 0 & \text{in } \Omega, \\ \dfrac{\partial u_*^{(l)}}{\partial \nu} = g^{(l)} & \text{on } \partial\Omega, \end{cases} \tag{1.2}$$

where $g^{(l)}$ are N given functions and ω is the operating angular frequency. The wavelength λ in the background medium is given by $\lambda := 2\pi/\omega$.

*Received by the editors September 20, 2010; accepted for publication (in revised form) January 7, 2013; published electronically April 3, 2013. This work was partially supported by ERC Advanced Grant Project MULTIMOD–267184, National Institute for Mathematical Sciences (2010 Thematic Program, TP1003), Korea Research Foundation grant KRF-2008-220-C00002, and NRF grants 2009-0090250, 2009-0085987, and 2010-0017532.

http://www.siam.org/journals/sicon/51-2/80895.html

†Department of Mathematics and Applications, Ecole Normale Supérieure, 75005 Paris, France (habib.ammari@ens.fr).

‡Department of Mathematics, Stanford University, Stanford, CA 94305 (pgarapon@stanford.edu).

§Laboratoire J.L. Lions, Université Paris VII, 75252 Paris, France (jouve@math.jussieu.fr).

¶Department of Mathematics, Inha University, Incheon 402-751, Korea (hbkang@inha.ac.kr).

‖Department of Mathematical Sciences, Korean Advanced Institute of Science and Technology, Daejeon 305-701, Korea (mklim@kaist.ac.kr, shyu@kaist.ac.kr).

To fix our ideas, we use, as an example, plane waves to identify the inclusion. We choose

$$g^{(l)}(x) := \frac{\partial}{\partial \nu} e^{i\omega\theta_l \cdot x} = i\omega\theta_l \cdot \nu(x) e^{i\omega\theta_l \cdot x} \quad \text{on } \partial\Omega, \quad l = 1, \ldots, N, \tag{1.3}$$

where $\{\theta_1, \ldots, \theta_N\}$ is a set of N unit directions uniformly distributed on the unit sphere S^{d-1}.

We assume that the size of D_* and the distance between D_* and $\partial\Omega$ are large compared to the wavelength λ. Throughout this paper, we say that a target is extended if its characteristic size is of order of or larger than half the operating wavelength λ. The inverse problem considered in this paper is to reconstruct the extended inclusion D_* from the boundary measurements $(u_*^{(l)})_{l=1}^N$ on $\partial\Omega$, where, for $l = 1, \ldots, N$, $u_*^{(l)}$ is the solution of (1.2) with $g^{(l)}$ given by (1.3).

With an infinite number of measurements, a uniqueness result for the inverse problem under consideration has been proved by Isakov [24].

The Helmholtz equation (1.2) is a mathematical model for acoustical and microwave soundings of biological media [1]. The function $u_*^{(l)}$ denotes the pressure or the voltage potential, respectively. The reconstruction problem is known to be, in general, severely ill-posed. However, if the inclusions are small compared to the operating wavelength, then one can design, using asymptotic methods, quite accurate and robust imaging algorithms. Small inclusion imaging has been the subject of important analytical and numerical studies; see, for instance, [1, 2, 6, 7, 8, 9, 12]. The developed algorithms are direct, i.e., noniterative.

Since, in the case of extended inclusions considered here the data structure is quite complicated, a direct imaging approach cannot be developed. However, as will be shown in this paper, direct approaches can be used to construct a good initial guess.

The main objective of this paper is to propose a new regularized optimal control approach for recovering the extended inclusion D_* from the boundary measurements. A standard approach is to minimize the L^2-discrepancy between the measured and computed data using a least-squares formulation. One can use total variation regularization to recover sharp discontinuities. The computation of the shape derivative of the L^2-discrepancy shows that a filtering effect is the main difficulty in solving this inverse problem.

The main novelty of our paper is the establishment of a regularized optimization approach that yields better imaging in the sense of resolution and stability. More important, we provide an optimal representation of the inclusion shape. We also prove a local Lipschitz stability result for reconstructing the inclusion. We then show results of computational experiments to demonstrate the efficiency of the proposed regularization. To handle topology changes such as breaking one component into two, we develop a level set version of our approach. Our results in this paper provide mathematical interpretations of important physical notions such as the resolution limit, the stability, and the shape representations in wave imaging.

The paper is organized as follows. In section 2 we present the first standard algorithm for solving the reconstruction problem. In section 3 we propose our new algorithm and provide an optimal shape representation. Local stability results are formulated and proved in section 4. In section 5 we discuss a MUSIC (multiple signed classification)-type algorithm to get a good initial guess. Section 6 is devoted to a level set version of our algorithm. Some numerical simulations for testing the proposed regularized optimal control approach are presented in section 7. The paper

ends with a discussion in section 8. Some results on the filtering property of the Helmholtz equation are given in Appendices A and B. Our results are generalized to linear elasticity in Appendix C. A discrete version of the method proposed in this paper has been adapted in [4] for multistatic imaging of extended targets.

2. First approach. The first (standard) approach to solving the inverse problem is to minimize over D the following cost functional:

$$J[D] := \frac{1}{2}\sum_{l=1}^{N}\int_{\partial\Omega}\left|u^{(l)}[D]-u_*^{(l)}\right|^2\,d\sigma, \tag{2.1}$$

where $u^{(l)}[D]$ is the solution to

$$\begin{cases} \nabla\cdot\gamma_D\nabla u^{(l)}+\omega^2u^{(l)}=0 & \text{in } \Omega,\\ \dfrac{\partial u^{(l)}}{\partial\nu}=g^{(l)} & \text{on } \partial\Omega. \end{cases} \tag{2.2}$$

Here, $\gamma_D = 1+(k-1)\chi[D]$.

It is known that minimizing (2.1) is ill-posed [20, 28, 38]. One can regularize the problem by minimizing over D the regularized cost functional:

$$J_{\text{reg}}[D] := \frac{1}{2}\sum_{l=1}^{N}\int_{\partial\Omega}|u^{(l)}[D]-u_*^{(l)}|^2\,d\sigma+\rho TV(\gamma_D),$$

where ρ is the regularization parameter and TV is the total variation defined for $q\in L^1$ by

$$TV(q) := \sup\left\{\int_\Omega q\nabla\cdot g\,dx : g\in\mathcal{C}_0^1(\Omega)^d,\ |g(x)|\le 1 \text{ for all } x\in\Omega\right\}.$$

Here $|\cdot|$ is the Euclidean norm of a vector. The regularization by total variation was introduced in [17, 18] for the purpose of obtaining sharp images of the discontinuity.

Suppose that $-\omega^2$ is not an eigenvalue of $-\nabla\cdot\gamma_D\nabla$ in Ω with homogeneous Neumann boundary conditions. For a given function h on ∂D, the shape derivative $d_{\mathcal{S}}J[D]$ of $J[D]$ is given for h of class $\mathcal{C}^1$ by

$$(d_{\mathcal{S}}J[D],h) = \sum_{l=1}^{N}\Re e\int_{\partial\Omega}(u^{(l)}[D]-u_*^{(l)})\overline{v^{(l)}[h]}\,d\sigma, \tag{2.3}$$

where $v^{(l)}[h]$ is the solution to

$$\begin{cases} \Delta v^{(l)}+\omega^2v^{(l)}=0 & \text{in } \Omega\setminus\overline{D},\\ k\Delta v^{(l)}+\omega^2v^{(l)}=0 & \text{in } D,\\ v^{(l)}|_+-v^{(l)}|_-=(k-1)h\dfrac{\partial u^{(l)}[D]}{\partial\nu}\Big|_- & \text{on } \partial D,\\ \dfrac{\partial v^{(l)}}{\partial\nu}\Big|_+-k\dfrac{\partial v^{(l)}}{\partial\nu}\Big|_-=(k-1)\dfrac{\partial}{\partial T}\left(h\dfrac{\partial u^{(l)}[D]}{\partial T}\right) & \text{on } \partial D,\\ \dfrac{\partial v^{(l)}}{\partial\nu}=0 & \text{on } \partial\Omega. \end{cases} \tag{2.4}$$

Here the subscripts $\pm$ indicate the limit from outside and inside D, $T(x)$ denotes the unit tangent vector at x on ∂D, and $\partial/\partial T$ stands for the tangential derivative. By abuse of notation, we denote by ν the outward normal to ∂D. We restrict the consideration to two dimensions for simplicity (extension to three dimensions is apparent). The proof of (2.3) follows immediately from [14, Theorem 1.2]. Note that the shape derivative is derived here under assumptions which do not allow topology changes.

To explicitly compute the shape derivative of J, we introduce the adjoint state $p^{(l)}[D]$ as the solution to

$$\begin{cases} \nabla \cdot \gamma_D \nabla p^{(l)}[D] + \omega^2 p^{(l)}[D] = 0 & \text{in } \Omega, \\ \dfrac{\partial p^{(l)}[D]}{\partial \nu} = (u^{(l)}[D] - u_*^{(l)}) & \text{on } \partial\Omega. \end{cases} \tag{2.5}$$

Introduce $N^\omega[D](x,y)$ as the Green function for $\nabla \cdot \gamma_D \nabla + \omega^2$ in Ω corresponding to a Dirac mass at y with homogeneous Neumann boundary conditions on $\partial\Omega$. That is, N^ω is the unique solution to

$$\begin{cases} (\nabla_x \cdot \gamma_D \nabla_x + \omega^2) N^\omega[D](x,y) = -\delta_y & \text{in } \Omega, \\ \dfrac{\partial N^\omega[D]}{\partial \nu}\Big|_{\partial\Omega} = 0 & \text{on } \partial\Omega. \end{cases} \tag{2.6}$$

It is easy to verify that $N^\omega[D](x,y) = N^\omega[D](y,x)$ for all $x \neq y \in \Omega$. See, for instance, [10, p. 26]. Note that $p^{(l)}[D]$ and $v^{(l)}[h]$ can be written as

$$p^{(l)}[D](x) = \int_{\partial\Omega} (u^{(l)}[D] - u_*^{(l)})(y) N^\omega[D](x,y)\, d\sigma(y)$$

and (see, for instance, [10, p. 59])

$$v^{(l)}[h](x) = \int_{\partial D} h(y) M(y) \nabla u^{(l)}[D](y) \cdot \nabla_y N^\omega[D](x,y)\, d\sigma(y),$$

where

$$M(y) := (k-1)(k\nu(y) \otimes \nu(y) + T(y) \otimes T(y)) \quad \text{for } y \in \partial D.$$

Now, using $p^{(l)}[D]$ to express the integral

$$\int_{\partial\Omega} (u^{(l)}[D] - u_*^{(l)}) \overline{v^{(l)}[h]}\, d\sigma,$$

we find that $d_{\mathcal{S}} J[D]$ in the direction of $h\nu$ is given by

$$(d_{\mathcal{S}} J[D], h) = (k-1) \int_{\partial D} h\, \Re e \sum_{l=1}^{N} \left(k \frac{\partial p^{(l)}[D]}{\partial \nu}\Big|_- \frac{\partial \overline{u^{(l)}[D]}}{\partial \nu}\Big|_- + \frac{\partial p^{(l)}[D]}{\partial T} \frac{\partial \overline{u^{(l)}[D]}}{\partial T} \right) d\sigma. \tag{2.7}$$

Set

$$w[D] = \Re e \sum_{l=1}^{N} \left(k \frac{\partial p^{(l)}[D]}{\partial \nu}\Big|_- \frac{\partial \overline{u^{(l)}[D]}}{\partial \nu}\Big|_- + \frac{\partial p^{(l)}[D]}{\partial T} \frac{\partial \overline{u^{(l)}[D]}}{\partial T} \right). \tag{2.8}$$

A simple algorithm for minimizing (2.1) consists of replacing, in each step,

$$\partial D \mapsto \partial D + h\nu,$$

where

$$h = -J[D]\frac{w[D]}{(d_{\mathcal{S}}J[D], w[D])} = -J[D]\frac{w[D]}{(k-1)\int_{\partial D} w[D]^2}\, d\sigma. \tag{2.9}$$

This algorithm is nothing other than a solution of $J[D] = 0$ by the Newton method. Note that the first fraction is meant to be the pseudoinverse of the operator $d_{\mathcal{S}}J[D]$ with respect to $L^2(\partial D)$.

3. Second approach. For the first approach, $d_{\mathcal{S}}J[D]$ acts like a filter of the oscillations in the shape changes. Roughly speaking, write $h = h_{\text{low}} + h_{\text{high}}$, where h_{low} and h_{high} are, respectively, the low- and high-frequency components of h.

Fix the threshold to separate the high-frequency component of h from the low-frequency one by

$$\frac{||\partial h_{\text{high}}/\partial T||_{L^2(\partial D)}}{||h_{\text{high}}||_{L^2(\partial D)}} > \beta. \tag{3.1}$$

One can see that there exists β_0 such that for $\beta \geq \beta_0$,

$$\int_{\partial D} h_{\text{high}}\, w[D]\, d\sigma \approx 0, \tag{3.2}$$

which shows that h_{high} cannot be reconstructed from boundary measurements. In other words, the cost functional is almost invariant with respect to highly oscillatory variations so that the shape boundary can be reconstructed only up to oscillatory parts. Therefore, the minimization of the cost functional (2.1) leads to images with limited resolution. We refer the reader to Appendix A for a quick check of (3.2).

In order to enhance the resolution, one should allow the adjoint state $p^{(l)} = p^{(l)}[D]$ to be in a richer space than the space spanned by the solutions of (2.5). Note that $p^{(l)}$ is given by

$$p^{(l)} = \Lambda_D((u^{(l)}[D] - u_*^{(l)})) \quad \text{for } l = 1, \ldots, N,$$

where the operator $\Lambda_D : L^2(\partial\Omega) \to L^2(\partial D)$ is defined by

$$\Lambda_D(f) = p|_{\partial D},$$

with

$$\begin{cases} \nabla \cdot \gamma_D \nabla p + \omega^2 p = 0 & \text{in } \Omega, \\ \dfrac{\partial p}{\partial \nu} = f & \text{on } \partial\Omega. \end{cases} \tag{3.3}$$

It is easy to see that the adjoint $\Lambda_D^* : L^2(\partial D) \to L^2(\partial\Omega)$ is given for $v \in L^2(\partial D)$ by

$$\Lambda_D^*(v) = w|_{\partial\Omega},$$

where w is the solution to

$$\begin{cases} \Delta w + \omega^2 w = 0 & \text{in } \Omega \setminus \overline{D}, \\ k\Delta w + \omega^2 w = 0 & \text{in } D, \\ kw|_+ = w|_- & \text{on } \partial D, \\ \dfrac{\partial w}{\partial \nu}\Big|_- - \dfrac{\partial w}{\partial \nu}\Big|_+ = v & \text{on } \partial D, \\ \dfrac{\partial w}{\partial \nu} = 0 & \text{on } \partial\Omega. \end{cases} \tag{3.4}$$

Here, ν denotes the outward normal to ∂D. Note that the transmission conditions in (3.4) are dual to those satisfied by the solution p of (3.3). In order to verify (3.4), we multiply it by p and integrate by parts to find that

$$\begin{aligned} \int_{\partial\Omega} f\overline{w}\, d\sigma &= \int_{\partial D} p\left(\frac{\partial \overline{w}}{\partial \nu}\Big|_+ - \frac{\partial \overline{w}}{\partial \nu}\Big|_-\right) d\sigma - \int_{\partial D}\left(\frac{\partial p}{\partial \nu}\Big|_+ \overline{w}_+ - \frac{\partial p}{\partial \nu}\Big|_- \overline{w}_-\right) d\sigma \\ &= \int_{\partial D} p\overline{v}\, d\sigma - \int_{\partial D} \frac{\partial p}{\partial \nu}\Big|_- \left(k\overline{w}_+ - \overline{w}_-\right) d\sigma \\ &= \int_{\partial D} p\overline{v}\, d\sigma. \end{aligned}$$

Let $\{f_i[D] : i = 1, \ldots, M\}$ be an orthonormal basis of the image space of $\Lambda_D^*\Lambda_D$ after truncating "small" eigenvalues of $\Lambda_D^*\Lambda_D$. The threshold for such a truncation is fixed in terms of the signal-to-noise ratio in the measured data and depends on the size of D and the distance from D to the boundary $\partial\Omega$. See [5] and Appendix B.

It is worthwhile to notice that the integral kernel of $\Lambda_D^*\Lambda_D$ is given by

$$\int_{\partial D} N^\omega[D](x,z)\overline{N^\omega[D](z,y)}\, d\sigma(z), \quad x, y \in \partial\Omega, \tag{3.5}$$

because Λ_D is given by

$$\Lambda_D(f)(x) = \int_{\partial\Omega} f(y) N^\omega[D](x,y)\, d\sigma(y), \quad x \in \partial D, \tag{3.6}$$

and hence

$$\Lambda_D^*(v)(x) = \int_{\partial D} v(y)\overline{N^\omega[D](x,y)}\, d\sigma(y), \quad x \in \partial\Omega. \tag{3.7}$$

Instead of minimizing the L^2-norm of the discrepancy between the measurements and the computed data, $u^{(l)}[D] - u_*^{(l)}$ for $l = 1, \ldots, N$, as in the first optimization procedure, we minimize the L^2-norm of the projection of $u^{(l)}[D] - u_*^{(l)}$ onto the space spanned by $\{f_i[D] : i = 1, \ldots, M\}$ in order to generate the highest possible oscillations in the adjoint states and, consequently, get optimal reconstruction of the shape changes h. This can be done only by changing the optimization procedure. Indeed, since the orthonormal basis $\{f_i[D] : i = 1, \ldots, M\}$ depends on D, at each step one should change the minimization cost functional.

Our new algorithm minimizes the following cost functional at each step $n \geq 1$ over all possible shape changes δD:

$$\mathcal{J}_n[\delta D] := \frac{1}{2}\sum_{l=1}^{N}\sum_{i=1}^{M}\left|\int_{\partial\Omega}(u^{(l)}[D_{n-1}+\delta D]-u_*^{(l)})\overline{f_i[D_{n-1}]}\,d\sigma\right|^2, \tag{3.8}$$

where D_0 is an initial guess and $u^{(l)}[D_{n-1}+\delta D]$ is the solution to (2.2) with $D := D_{n-1}+\delta D$. For minimizing the cost functional, we perform just a single Newton step. Note that at each step n, $\mathcal{J}_n$ is an L^2-projection of the discrepancy between the computed and the measured data onto the space spanned by $\{f_i[D_{n-1}] : i = 1,\dots,M\}$.

For fixed n, we will make only one iteration in order to minimize $\mathcal{J}_n$. We modify the shape D_{n-1} to obtain $D_{n-1}+\delta D_n$ by solving $\mathcal{J}_n[D_n]=0$ by a Newton method.

Our algorithm can be interpreted as a two-step algorithm. First, one linearizes the problem, and then one projects the data over an optimal basis that ensures stability and gives optimal representation of the shape changes (see section 4 for details). It is clear that one has to change the cost functional at each step because of the inherent nonlinearity of the inverse problem of reconstructing the inclusion from boundary measurements.

To find δD_n, one can compute the shape derivative of the cost functional $\mathcal{J}[D]$ given by

$$\mathcal{J}[D] := \frac{1}{2}\sum_{l=1}^{N}\sum_{i=1}^{M}\left|\int_{\partial\Omega}(u^{(l)}[D]-u_*^{(l)})\overline{f_i}\,d\sigma\right|^2,$$

in the direction of $h\nu$, where the functions f_i are given as $f_i[D_{n-1}]$. In fact,

$$\mathcal{J}_n[\delta D_n] \approx \mathcal{J}[D_{n-1}] + (d_{\mathcal{S}}\mathcal{J}[D_{n-1}], h_n),$$

with δD_n being chosen to have the form

$$\delta D_n := \Big\{h_n(x)\nu(x),\ x\in\partial D_{n-1}\Big\}.$$

Similarly to (2.3), we obtain that

$$(d_{\mathcal{S}}\mathcal{J}[D], h) = \sum_{l=1}^{N}\sum_{i=1}^{M}\Re e\left[\int_{\partial\Omega}(u^{(l)}[D]-u_*^{(l)})\overline{f_i}\,d\sigma\int_{\partial\Omega}\overline{v^{(l)}[h]}f_i\,d\sigma\right], \tag{3.9}$$

where $v^{(l)}[h]$ is given by (2.4).

Let $p_i[D]$ be the solution to

$$\begin{cases} \nabla\cdot\gamma_D\nabla p_i + \omega^2 p_i = 0 & \text{in } \Omega,\\ \dfrac{\partial p_i}{\partial\nu} = f_i & \text{on } \partial\Omega. \end{cases} \tag{3.10}$$

Then we have from (2.4)

$$\int_{\partial\Omega}\overline{v^{(l)}[h]}f_i\,d\sigma = (k-1)\int_{\partial D} h\left(k\frac{\partial p_i[D]}{\partial\nu}\Big|_- \frac{\partial\overline{u^{(l)}[D]}}{\partial\nu}\Big|_- + \frac{\partial p_i[D]}{\partial T}\frac{\partial\overline{u^{(l)}[D]}}{\partial T}\right)d\sigma.$$

Set

$$\alpha_{il}[D] := (k-1)\int_{\partial\Omega}(u^{(l)}[D]-u_*^{(l)})\overline{f_i}[D]\,d\sigma, \quad i=1,\dots,M,\ l=1,\dots,N, \tag{3.11}$$

and

$$w_i^{(l)}[D] := k\frac{\partial p_i[D]}{\partial\nu}\Big|_- \frac{\partial\overline{u^{(l)}[D]}}{\partial\nu}\Big|_- + \frac{\partial p_i[D]}{\partial T}\frac{\partial\overline{u^{(l)}[D]}}{\partial T}. \tag{3.12}$$

Then (3.9) can be rewritten as

$$(d_{\mathcal{S}}\mathcal{J}[D],h) = \Re e\sum_{l=1}^{N}\sum_{i=1}^{M}\alpha_{il}[D_{n-1}]\int_{\partial D} h w_i^{(l)}[D_{n-1}]\,d\sigma. \tag{3.13}$$

Thus, in exactly the same way as in (2.9), the update δD_n is chosen as follows:

$$h_n = -\frac{\mathcal{J}[D_{n-1}]}{\sum_{i,l}\left((d_S\mathcal{J}[D_{n-1}], w_i^{(l)}[D_{n-1}])\right)^2}\sum_{i,l}(d_S\mathcal{J}[D_{n-1}], w_i^{(l)}[D_{n-1}])\, w_i^{(l)}[D_{n-1}]. \tag{3.14}$$

Here, $(d_S\mathcal{J}[D_{n-1}], w_i^{(l)}[D_{n-1}])$ is computed using formula (3.13). Note also that

$$p^{(l)} = \Lambda_D((u^{(l)}[D]-u_*^{(l)})) \approx \sum_{i=1}^{M}\lambda_i((u^{(l)}[D]-u_*^{(l)}), f_i)p_i, \tag{3.15}$$

where λ_i^2 is the eigenvalue of $\Lambda_D^*\Lambda_D$ corresponding to f_i, and therefore, h_n corresponds to back-propagating the projections of the functions $u^{(l)}-u_*^{(l)}$ onto the space spanned by the functions f_i for $i=1,\dots,M$. Note that by back-propagating a boundary datum on $\partial\Omega$ we mean solving the Helmholtz equation with the inclusion D. Note also that one should constrain the change δD_n to be sufficiently small so that $D_{n-1}+\delta D_n \subset \Omega$.

The described algorithm filters $d_{\mathcal{S}}\mathcal{J}$ given by (2.7) at each step, with an optimal filter constructed through a singular value decomposition of the operator Λ_D. In other words, while in the standard approach the adjoint state corresponds to back-propagation of the discrepancy, in the new regularized approach the discrepancy is projected onto an optimal basis at each step ($\{f_i[D_{n-1}]\}$ at step n), and only the elements of this optimal basis are back-propagated inside the domain. The traces of the back-propagated functions on the boundary of the inclusion at step n form a basis to represent the changes in the shape in order to evolve it. This yields better resolution and stability properties. However, there is a trade-off between resolution and stability. To gain resolution one has to choose M as high as possible. But if it is too high, then it follows from the form of the coefficients α_{il} in (3.11) and the fact that f_i is highly oscillating for large i that the algorithm is unstable in the case of noisy data $(u_*^{(l)})_{l=1,\dots,N}$. Note that $M=\infty$ yields exactly a scheme for (2.1) without regularization. On the other hand, when M is small there are savings in computational effort.

Note also that our algorithm extends as well to the case where the inclusion is perfectly insulating or the case where conducting. In these two cases, according to [29], the analogues of $\Lambda_D^*\Lambda_D$ are exactly those used in the factorization method.

Finally, it is worth noticing that the basis $\{f_i\}$ can be updated by using the leading-order term in the asymptotic expansion of $f_i[D+\delta D]$ in terms of δD, which has been obtained in [12]. However, to avoid error accumulation, the basis should be recomputed after a few steps.

4. A local stability result. Let $\mathcal{V}[D]$ be the (finite-dimensional) vector space spanned by $\Im m\, w_i^{(l)}$ and $\Re e\, w_i^{(l)}$ for $l = 1, \ldots, N$ and $i = 1, \ldots, M$, where $w_i^{(l)}$ is defined by (3.12). As we said previously, the number M is fixed in terms of the signal-to-noise ratio in the measured data.

From section 3, it follows that an optimal representation of small changes in D is as follows:

$$\delta D := \left\{ h(x)\nu(x),\ x \in \partial D \right\}, \quad h \in \mathcal{V}[D].$$

This representation is optimal in the sense that any component of the changes δD in the space orthogonal to $\mathcal{V}[D]$ in $L^2(\partial D)$ cannot be reconstructed, which can be immediately seen from (3.13). In other words, choosing any other basis than $\mathcal{V}[D]$ is less efficient. Moreover, as will be shown by Proposition 4.1, the reconstruction of the components of δD that belong to $\mathcal{V}[D]$ is stable. Note that since D is of class $\mathcal{C}^{2,\eta}$ $(0 < \eta < 1)$, $\mathcal{V}[D]$ is a subset of $H^2(\partial D)$ because of the H^2-regularity of $w_i^{(l)}$ on ∂D; see, for instance, [22].

A natural representation of h is to expand it on a basis of $L^2(\partial D)$ (constructed, for instance, by solving the spectral problem for the Laplace–Beltrami operator). But, as shown previously, high oscillations in h cannot be reconstructed, which means that only the projection of h on the first basis (not highly oscillating) functions plays a role. However, there is no systematic way to set a threshold. From this point of view, the representation as a linear combination of elements of $\mathcal{V}[D]$ appears to be sparse, and the threshold is fixed in a systematic and optimal way.

A few components may be enough to represent all of the possible changes that could be reconstructed. Note also that the larger the distance between D_* and $\partial\Omega$ compared to the wavelength and the size of D_*, the smaller the dimension of $\mathcal{V}[D_*]$. If D_* is smaller than the wavelength $\lambda = 2\pi/\omega$, then the dimension of the vector space $\mathcal{V}[D_*]$ could be reduced to 1. In fact, in view of (3.5), we have

$$\begin{aligned}\Lambda_D^*\Lambda_D(f)(x) &= |\partial D| \int_{\partial\Omega} f(y) N^\omega[D](y,z)\, d\sigma(y) \overline{N^\omega[D](z,x)} + o(|\partial D|)\\ &= |\partial D| \int_{\partial\Omega} f(y) N^\omega(y,z)\, d\sigma(y) \overline{N^\omega(z,x)} + o(|\partial D|), \quad x \in \partial\Omega,\end{aligned}$$

where z is a point in D and $N^\omega(z,x)$ is the Green function for $\Delta + \omega^2$, with homogeneous Neumann boundary conditions on Ω (without inclusion). Here $|\partial D|$ denotes the surface of ∂D. It shows that the significant eigenvalue of $\Lambda_D^*\Lambda_D$ is $|\partial D|\ \|N^\omega\|^2_{L^2(\partial\Omega)}$ and corresponding eigenvector is $N^\omega(\cdot, z)$.

The stability of the reconstruction of the components of the changes that are in $\mathcal{V}[D]$ can be stated mathematically by introducing a measure of arbitrarily small changes δD in D. This can be done by setting

$$|\delta D|^2 = \sum_{i,l} \left| \int_{\partial D} h w_i^{(l)}\, d\sigma \right|^2 + \left| \int_{\partial D} \frac{\partial h}{\partial T} \frac{\partial w_i^{(l)}}{\partial T}\, d\sigma \right|^2. \tag{4.1}$$

We emphasize that since $\mathcal{V}[D]$ is finite-dimensional, all the norms are equivalent, and therefore the quantities

$$\sum_{i,l}\left|\int_{\partial D} hw_i^{(l)}\,d\sigma\right|^2 \quad \text{and} \quad \sum_{i,l}\left|\int_{\partial D}\frac{\partial h}{\partial T}\frac{\partial w_i^{(l)}}{\partial T}\,d\sigma\right|^2$$

are of the same order (independently of h). Hence, we have

$$|\delta D|^2 \approx \sum_{i,l}\left|\int_{\partial D} hw_i^{(l)}\,d\sigma\right|^2.$$

Note also that the oscillations in $w_i^{(l)}$ are limited and that they are functions of ω and the distance between D and $\partial\Omega$. As in (3.1), the oscillations in $w_i^{(l)}$ can be measured by the quotient

$$\frac{\||\partial w_i^{(l)}/\partial T||_{L^2(\partial D)}}{||w_i^{(l)}||_{L^2(\partial D)}}. \tag{4.2}$$

By Shannon's sampling theorem (see, for instance, [31, p. 41]) this yields an estimate of the resolution limit, δ_{res}, when reconstructing small changes ∂D from boundary measurements:

$$\delta_{\text{res}} = 2\pi \min_{i,l}\frac{||w_i^{(l)}||_{L^2(\partial D)}}{\||\partial w_i^{(l)}/\partial T||_{L^2(\partial D)}}. \tag{4.3}$$

Hence, any detail in the perturbations of size $\delta < \delta_{\text{res}}$ cannot be represented by functions in $\mathcal{V}[D]$ since it has oscillations higher than any function in $\mathcal{V}[D]$.

Now, from [12], one can prove that if $\delta D := \{h(x)\nu(x), x \in \partial D\}$ with $||h||_{\mathcal{C}^1(\partial D)}$ small enough, then

$$u^{(l)}[D+\delta D] - u^{(l)}[D] = v^{(l)}[h] + O(||h||^d_{\mathcal{C}^1(\partial D)}) \tag{4.4}$$

uniformly on $\partial\Omega$, with d being the space dimension. Moreover,

$$\|v^{(l)}[h]\|_{L^2(\partial\Omega)} = O(||h||^{d-1}_{\mathcal{C}^1(\partial D)}). \tag{4.5}$$

The expansion (4.4) yields

$$\int_{\partial\Omega}(u^{(l)}[D+\delta D] - u^{(l)}[D])\overline{f_i}[D]\,d\sigma = (k-1)\int_{\partial D}\overline{hw_i^{(l)}[D]}\,d\sigma + O(||h||^d_{\mathcal{C}^1(\partial D)}).$$

Thus, from (4.5) it follows that

$$|\delta D|^2 \approx \frac{1}{(k-1)^2}\sum_{l=1}^{N}\sum_{i=1}^{M}\left|\int_{\partial\Omega}(u^{(l)}[D+\delta D] - u^{(l)}[D])\overline{f_i}[D]\,d\sigma\right|^2 + O(||h||^{2d-1}_{\mathcal{C}^1(\partial D)}).$$

Therefore, the following local stability result holds.

PROPOSITION 4.1. *Suppose that $\delta D := \{h(x)\nu(x), x \in \partial D\}$ with $||h||_{\mathcal{C}^1(\partial D)} < \epsilon$. Define the measure $|\delta D|$ by* (4.1). *Then there exists a positive constant C such that for $\epsilon < \epsilon_0$,*

$$|\delta D|^2 \le C\left(\sum_{l=1}^{N}\sum_{i=1}^{M}\left|\int_{\partial\Omega}(u^{(l)}[D+\delta D] - u^{(l)}[D])\overline{f_i}[D]\,d\sigma\right|^2 + \epsilon^{2d-1}\right). \tag{4.6}$$

The estimate (4.6) shows local Lipschitz stability of the reconstruction (up to ϵ^{2d-1}) and uniqueness in the class of perturbations in $\mathcal{V}[D]$. In fact, fix ϵ to be a positive small parameter. Suppose we have D_1 and D_2 such that $D_2 = D_1 + \delta D$ for some changes $\delta D := \{h(x)\nu(x), x \in \partial D\}$ with $||h||_{\mathcal{C}^1(\partial D)} < \epsilon$. Then, up to $O(\epsilon^{d-1/2})$, $|\delta D|$ is bounded by $\sum_l \|u^{(l)}[D_1] - u^{(l)}[D_2]\|_{L^2(\partial\Omega)}$. This shows that the changes in $\mathcal{V}[D_1]$ can be reconstructed in a Lipschitz stable way. On the other hand, if

$$\int_{\partial\Omega} u^{(l)}[D_1]\overline{f_i}[D_1]\, d\sigma = \int_{\partial\Omega} u^{(l)}[D_2]\overline{f_i}[D_1]\, d\sigma, \quad l = 1, \ldots, N, \quad i = 1, \ldots, M,$$

and $\delta D \in \mathcal{V}[D_1]$, then

$$|\delta D|^2 \leq C\epsilon^{2d-1},$$

which shows that the normalized changes $\epsilon^{1-d}\delta D$ are approximately zero.

Proposition 4.1 indicates that the only information that can be reconstructed from the boundary measurements is the projection of ∂D onto the space $\mathcal{V}[D]$. Indeed, this reconstruction is stable. To the best of our knowledge, such a result is new. It describes an optimal solution for handling the ill-posedness character of the inverse problem of reconstructing an inclusion from boundary measurements. It gives the exact class where the detectable perturbations should be and ensures their reconstruction in a stable way. By linearization and projection, we have reduced the ill-posed inverse problem of reconstructing an extended inclusion to a family of well-posed problems in a much smaller, but at each step optimal, class in the sense of resolution and stability.

5. Initial guess by a MUSIC-type approach. There are many possible ways to get a good initial guess. One is to use a standard MUSIC-type projection approach. See, for instance, [23, 13, 11, 21, 30].

Let us consider the case of $g^{(l)} = \frac{\partial V^{(l)}}{\partial \nu}$, where $V^{(l)}$ is given by

$$V^{(l)}(x) = e^{i\omega\theta_l \cdot x} \quad \text{in } \Omega, \quad l = 1, \ldots, N.$$

We construct the response matrix $A = (A_{ll'})_{l,l'=1}^N$ with

$$A_{ll'} = \int_{\partial\Omega} u_*^{(l)} \frac{\partial \overline{V^{(l')}}}{\partial \nu}\, d\sigma - \int_{\partial\Omega} g^{(l)} \overline{V^{(l')}}\, d\sigma. \tag{5.1}$$

Integration by parts shows that

$$A_{ll'} = (1-k) \int_D \nabla u_*^{(l)} \cdot \nabla \overline{V^{(l')}}\, dx.$$

Let $c_1, \ldots, c_d$ be d unit independent vectors in $\mathbb{R}^d$. For z in the search region $\Omega' \subset\subset \Omega$, let

$$g_j(z) = (c_j \cdot \theta_1 e^{i\omega\theta_1 \cdot z}, \ldots, c_j \cdot \theta_N e^{i\omega\theta_N \cdot z})^t \quad \text{for } j = 1, \ldots, d,$$

where t denotes the transpose. We plot the MUSIC imaging functional

$$W(z) := \frac{1}{\sum_j ||(I-P)g_j(z)||} \quad \text{for } z \in \Omega', \tag{5.2}$$

where P is the orthogonal projection onto the range of the response matrix A. The set where $W(z)$ attains its highest values would be a good initial guess for D_*; see [11, 25].

To understand this, divide the domain D into a set of small elements $\mathcal{O}_n$. Then using the rectangular quadrature rule yields

$$A_{ll'} \approx (1-k)\sum_n \theta_{l'} \cdot \int_{\mathcal{O}_n} \nabla u^{(l)}(x)dx\, e^{i\omega\theta_{l'}\cdot y_n},$$

where $y_n \in \mathcal{O}_n$. Therefore, the only points $z \in \Omega$ such that $g_j(z), j = 1, \ldots, d$, are in the range of A are those inside D.

According to the Rayleigh resolution limit, any detail less than one half of the wavelength cannot be seen [1]. By dividing the search domain Ω' into pixels of length of the order of half the wavelength, only one point at each pixel will contribute at the image space of the response matrix A. Each of these points can in principle be imaged using the MUSIC imaging functional. The resolution of the image provided by this technique is of the order of half the wavelength. Since the measurements are done at the boundary of Ω, a MUSIC-type image can be an initial guess, and by using the optimization algorithm described in the last section, higher resolution in imaging the inclusion can be achieved.

6. Level set framework. To handle topology changes such as breaking one component into two, we develop a level set version of our algorithm.

Within the level set framework, we represent ∂D as the zero level set of a continuous function ϕ so that $D = \{\phi < 0\}$. We convert the minimization problem (3.8) into a level set form by choosing the gradient ascent direction $F(x)$ as

$$F(x) = \Re e \sum_{l=1}^{N}\sum_{i=1}^{M} \alpha_{il}[D] w_i^{(l)}[D](x), \tag{6.1}$$

where α_{il} and $w_i^{(l)}$ are defined by (3.11) and (3.12), respectively.

Then we evolve ϕ by solving the Hamilton–Jacobi equation

$$\frac{\partial \phi}{\partial t} + F|\nabla\phi| = 0 \tag{6.2}$$

for one time step. We refer the reader to, for instance, [19, 26, 27, 35, 36].

We emphasize that in (6.1), F is defined only on the boundary ∂D, even though under the level set framework it has to be defined on the whole domain. We first note that since $\nu = \nabla\phi/|\nabla\phi|$, it follows that

$$\begin{aligned} w_i^{(l)}[D] &= (k-1)\left(\nabla p_i[D]\big|_- \cdot \frac{\nabla\phi}{|\nabla\phi|}\right)\left(\nabla\overline{u^{(l)}[D]}\big|_- \cdot \frac{\nabla\phi}{|\nabla\phi|}\right) + \nabla p_i[D]\big|_- \cdot \nabla\overline{u^{(l)}[D]}\big|_- \\ &= \left(\frac{1}{k}-1\right)\left(\nabla p_i[D]\big|_+ \cdot \frac{\nabla\phi}{|\nabla\phi|}\right)\left(\nabla\overline{u^{(l)}[D]}\big|_+ \cdot \frac{\nabla\phi}{|\nabla\phi|}\right) + \nabla p_i[D]\big|_+ \cdot \nabla\overline{u^{(l)}[D]}\big|_+. \end{aligned} \tag{6.3}$$

Therefore, (6.2) for ϕ can be modified as follows:

$$\begin{aligned} &\frac{\partial\phi}{\partial t} + \frac{1}{2}\Bigg(\Re e \sum_{l=1}^{N}\sum_{i=1}^{M} \alpha_{il}\left[\left(\frac{1}{k}-k\right)\mathrm{sgn}(\phi) + \frac{1}{k} + k - 2\right]\nabla p_i[D] \\ &\qquad \cdot \frac{\nabla\phi}{|\nabla\phi|}\nabla\overline{u^{(l)}[D]} \cdot \frac{\nabla\phi}{|\nabla\phi|}\Bigg)|\nabla\phi| \\ &\quad + \left(\Re e \sum_{l=1}^{N}\sum_{i=1}^{M} \alpha_{il}\nabla p_i[D] \cdot \nabla\overline{u^{(l)}[D]}\right)|\nabla\phi| = 0, \end{aligned} \tag{6.4}$$

where sgn is the sign function. The evolution of the level set function ϕ then follows from the solution of (6.4) instead of (6.2).

7. Numerical experiments. In this section we first show results of reconstructions using Method 2 (the second algorithm using (3.14)). We also show the results using Method 1 (the first standard algorithm using (2.9)) without regularization for comparison. Throughout this section, the background domain Ω is given by

$$\frac{x^2}{7^2} + \frac{y^2}{5^2} \leq 1,$$

and the conductivity inside the inclusion D is $k = 4$ and is assumed to be known. The angular frequency ω is 2, except in Example 3 where $\omega = 1$ is used as well.

The direct solver uses the boundary integral representation of the solution to (1.2). The number of nodal points on ∂D_* and $\partial\Omega$ is 128. At each iteration step n, we use 100 nodal points to uniformly discretize the boundary of the reconstructed inclusion D_n.

In the following examples, given the true inclusion D_*, we set $N = 20$ and compute the solution $u_*^{(l)}$ for $l = 1, \ldots, 20$, which satisfies

$$\nabla \cdot \gamma_{D_*} \nabla u_*^{(l)} + \omega^2 u_*^{(l)} = -\delta_{y_l} \quad \text{in } \mathbb{R}^2,$$

and also satisfies the outgoing radiation condition, where

$$y_l = 8(\cos((l-1)\pi/10),\ \sin((l-1)\pi/10)), \quad l = 1, \ldots, 20,$$

are point sources outside Ω. Clearly, $u_*^{(l)}|_\Omega$ is a solution to (1.2) with the Neumann datum $g^{(l)} = \partial u_*^{(l)}/\partial\nu$. We use $u_*^{(l)}|_{\partial\Omega}$ for $l = 1, \ldots, 20$ as input in the reconstruction algorithms, except in Figure 7.3, where we use $M = 10$.

Initial guess. To get an initial guess we use the MUSIC-type algorithm described in section 5. We collect the grid points where the MUSIC imaging functional W in (5.2) has a large value, and then find the smallest disk which encircles those grid points. We then modify the radius (among concentric disks) so that the L^2-discrepancy of $u[D]$ and u_* is minimal. Figure 7.1 shows results for two different inclusions. It clearly demonstrates that the MUSIC-type algorithm provides quite good initial guesses.

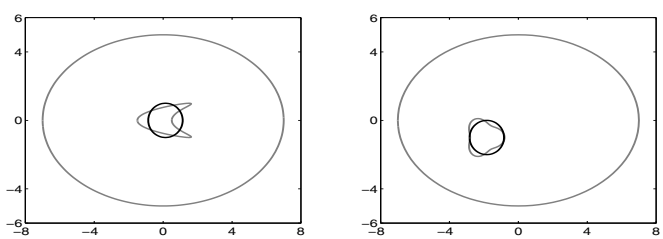

FIG. 7.1. *Initial guesses obtained by the MUSIC-type algorithm.*

Example 1. This example is for a reconstruction of the kite-shaped inclusion. We use the disk constructed above (the left figure in Figure 7.1) as the initial guess.

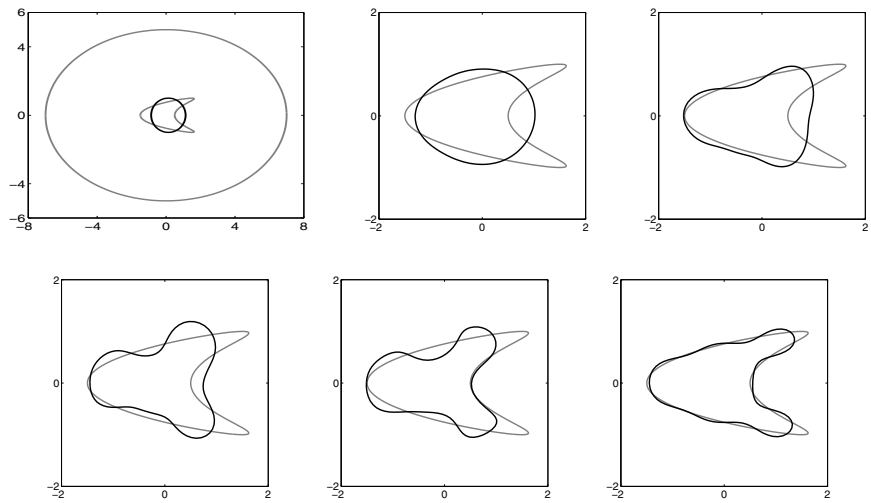

FIG. 7.2. *Reconstruction with Method* 2 *for* $M = 10$ *from measurements without error. The gray curve is the actual shape and the black curve is the reconstructed one. Images from top left to bottom right are the initial guess and the results of iterations* $1, \ldots, 4$. *The lower right image is the result of* 50 *iterations.*

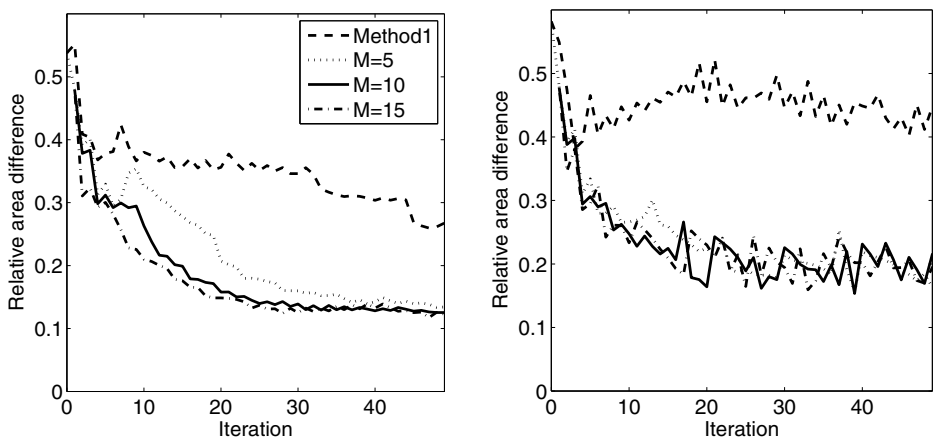

FIG. 7.3. *Graph of the relative area difference, i.e.,* $\frac{|D \Delta D_n|}{|D|}$. *The figure on the left is from data with* 0% *noise and on the right is from data with* 20% *relative noise. Method* 2 *gives better results with better stability.*

Figure 7.2 presents the initial guess and the shapes for five iterations using Method 2 without noise. It clearly shows how the shapes gradually approach the actual kite shape. Figure 7.3 compares the reconstruction results using Method 1 and Method 2 with 0% and 20% additive Gaussian noise, respectively (the percentage of noise is measured in terms of the L^2-norm). It shows that Method 2 gives better shape reconstruction results than Method 1, with better stability properties.

Example 2. In this example inclusions are unit disks perturbed by $h = 0.2\cos(m\theta)$ for $m = 3$ and 6. The inclusion is centered at $(-2, -1)$ in Figure 7.4 and at the origin in Figure 7.5. Figures 7.4 and 7.5 clearly show that Method 2 detects highly oscillatory perturbations of the shape better than Method 1. Here we use $\omega = 2$.

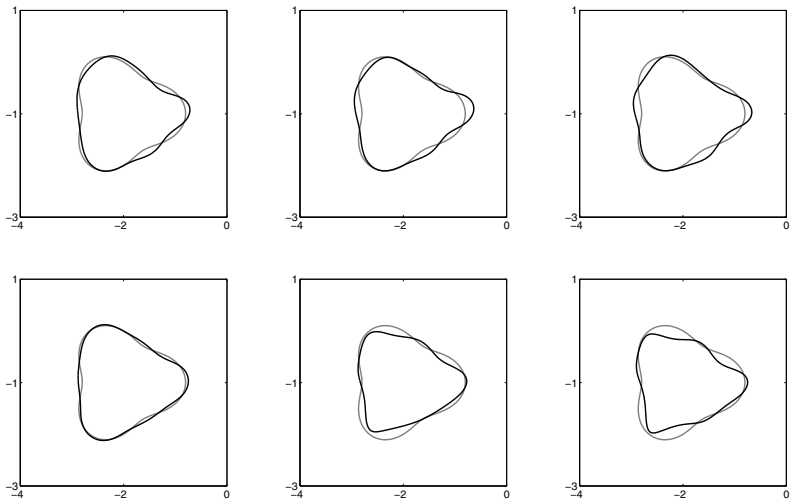

FIG. 7.4. *Reconstruction of the unit disk centered at* $(-2,-1)$ *perturbed by* $h = 0.2\cos(3\theta)$. *The upper row is obtained by using Method* 1 *and the lower row by Method* 2 *(after nine iterations). All three columns are reconstructions from data with* 0%, 10%, *and* 20% *noise.*

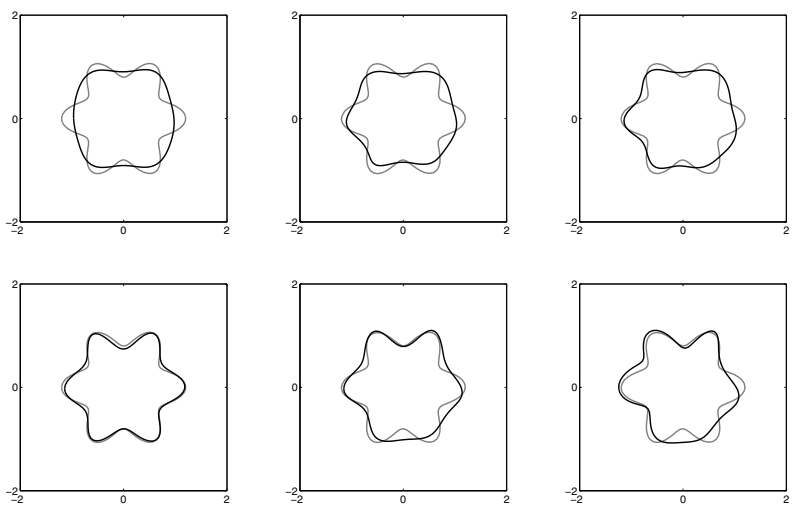

FIG. 7.5. *Reconstruction of the unit disk centered at the origin perturbed by* $h = 0.2\cos(6\theta)$. *The upper row is obtained by using Method* 1 *and the lower row by Method* 2 *(after nine iterations). All three columns are reconstructions from data with* 0%, 10%, *and* 20% *noise.*

Example 3. This example shows the role of the frequency in the reconstruction. Figure 7.6 shows the reconstruction results with Method 2 using $\omega = 1$ and $\omega = 2$ after 9 iterations. It shows that one cannot detect highly oscillatory parts of the shape by using low frequencies.

Example 4. This example shows a reconstruction of nonconvex shapes. Figure 7.7 shows that both Methods 1 and 2 work well for reconstruction of a mildly nonconvex shape and that Method 2 performs better. Figure 7.8 reveals the limitation of the reconstruction of severely nonconvex shapes.

It should be noted that because of numerical limitations of our code, $M = 10$ or $M = 15$ adds no extra accuracy to $M = 5$.

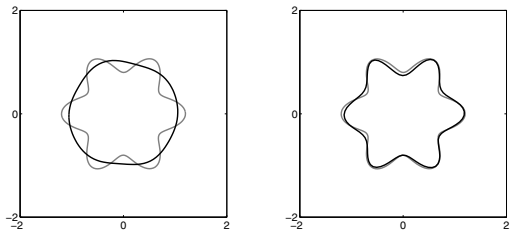

FIG. 7.6. *Images obtained after nine iterations with Method* 2 *from data without noise. The figure on the left is from data with* $\omega = 1$ *and the one on the right is from data with* $\omega = 2$. *Low-frequency data cannot detect high oscillations.*

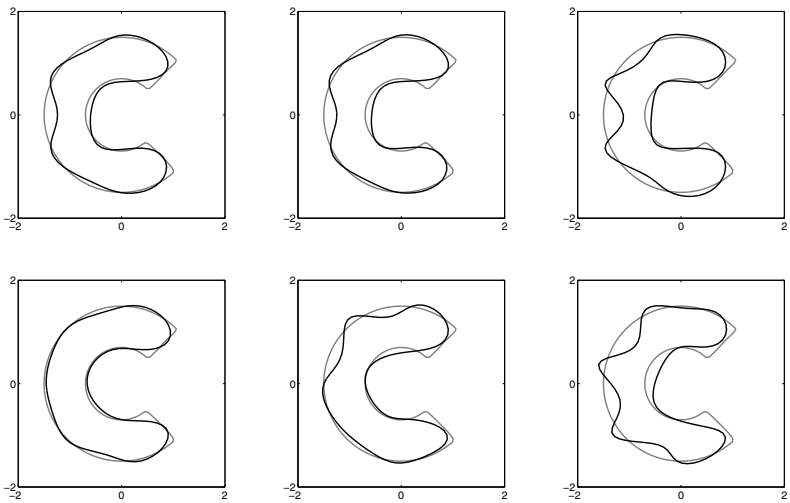

FIG. 7.7. *The upper row is the reconstruction with Method* 1 *and the second with Method* 2 *after* 21 *iterations. All three columns are the reconstructions from data with* $0\%, 10\%,$ *and* 20% *noise.*

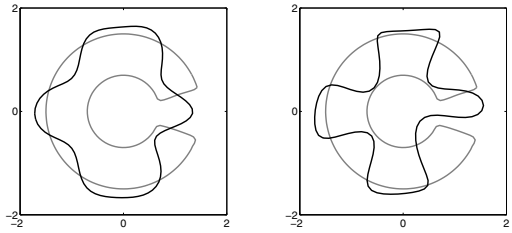

FIG. 7.8. *Reconstructed images after* 21 *iterations. The first and second figures are, respectively, obtained using Method* 1 *and* 2 *from data without noise. The figures reveal the limitation of Methods* 1 *and* 2 *for the shape reconstruction of severely nonconvex inclusions.*

We now show several reconstruction examples of multiple inclusions using the level set framework. The background domain, measurements, and initial guess are the same as above. We set the conductivity inside the inclusions to be identically 4 and the angular frequency to be $\omega = 2$ throughout this section.

Example 5. Figures 7.9 and 7.10 show that Method 2 in the level set framework successfully detects multiple inclusions.

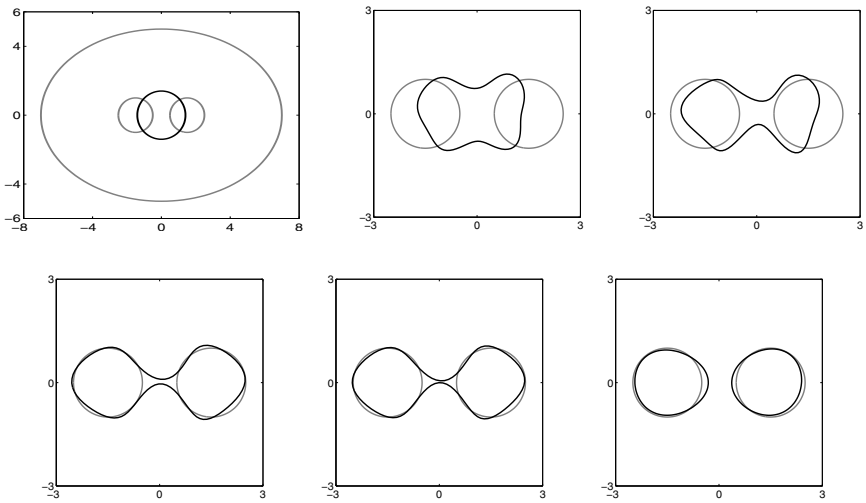

FIG. 7.9. *Reconstruction of multiple inclusions with Method* 2 *in the level set framework from measurements without noise. The gray curve is the actual shape and the black curve is the reconstructed one. Images are initial guess and those obtained after* 5, 10, 15, 16, *and* 19 *iterations, respectively.*

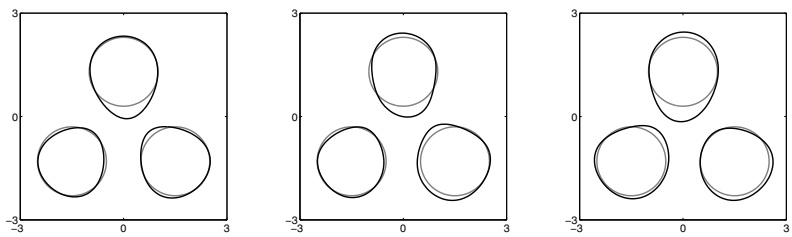

FIG. 7.10. *Reconstruction of multiple inclusions with Method* 2. *The first, second, and third are the reconstructions from data with* 0%, 10%, *and* 20% *noise after* 37, 42, *and* 53 *iterations, respectively.*

8. Concluding remarks. In this paper we have presented a new regularized optimal control approach for the reconstruction of inclusions from boundary measurements. We have constructed an optimal representation (in the sense of resolution and stability) of small changes in the shape of the inclusion and proved a local stability result. We have performed some numerical experiments to demonstrate the validity and the limitations of the proposed approach. The results clearly show that our approach is promising in recovering fine shape details.

To handle topology changes, we have developed a level set version of our approach. Our approach also extends to the reconstruction of elastic inclusions from boundary measurements.

Reconstruction of electromagnetic inclusions will be discussed in a forthcoming work. We also intend to generalize our inversion procedure to the case where only a part of the boundary is accessible.

Appendix A. High-frequency truncation. For simplicity, we restrict ourselves to the two-dimensional case. We parametrize ∂D by a 2π-periodic function s

proportional to the arclength. For a function h write the Fourier expansion of h,

$$h(s) = \frac{1}{\sqrt{2\pi}} \sum_{n\in\mathbb{Z}} \hat{h}_n e^{ins},$$

where

$$\hat{h}_n := \frac{1}{\sqrt{2\pi}} \int_{-\pi}^{\pi} h(s) e^{-ins}\, ds.$$

Now, because of the filtering properties of the Helmholtz equation (see [32, 33] and also Appendix B), for $w[D]$ defined by (2.8), there exists n_0 such that

$$w[D](s) \approx \sum_{|n|\le n_0} \hat{w}_n e^{ins}.$$

If one defines the high-frequency component of h by

$$h_{\text{high}} = \sum_{|n|>n_0} \hat{h}_n e^{ins},$$

then one can easily see that

$$\int_{\partial D} h_{\text{high}}\, w[D]\, d\sigma \approx 0.$$

Moreover, we have

$$\frac{||\partial h_{\text{high}}/\partial s||_{L^2(\partial D)}}{||h_{\text{high}}||_{L^2(\partial D)}} \ge n_0,$$

and hence n_0 is the threshold given in (3.1).

Appendix B. Singular value decomposition of the operator $\boldsymbol{\Lambda_D}$. Suppose that Ω and D are, respectively, the disks of center 0 and radii R and R' with $R' < R$. Write $f = \sum_n \hat{f}_n e^{in\theta}$, where θ is the angular variable. The explicit solution to (3.3), which can be rewritten in the polar coordinates as

$$\begin{cases} \left(\dfrac{k}{r}\dfrac{\partial}{\partial r} r \dfrac{\partial}{\partial r} + \dfrac{k}{r^2}\dfrac{\partial^2}{\partial \theta^2}\right) p + \omega^2 p = 0 & \text{in } D, \\ \left(\dfrac{1}{r}\dfrac{\partial}{\partial r} r \dfrac{\partial}{\partial r} + \dfrac{1}{r^2}\dfrac{\partial^2}{\partial \theta^2}\right) p + \omega^2 p = 0 & \text{in } \Omega \setminus \overline{D}, \\ p\big|_+ = p\big|_-, \quad \dfrac{\partial p}{\partial r}\Big|_+ = k \dfrac{\partial p}{\partial r}\Big|_- & \text{on } \partial D, \\ \dfrac{\partial p}{\partial r} = f & \text{on } \partial\Omega, \end{cases}$$

is given by

$$p(r,\theta) = \begin{cases} \sum_n (a_n J_n(\omega r) + b_n Y_n(\omega r)) e^{in\theta} & \text{in } \Omega \setminus \overline{D}, \\ \sum_n c_n J_n(\frac{\omega}{\sqrt{k}} r) e^{in\theta} & \text{in } D, \end{cases} \tag{B.1}$$

where the coefficients a_n, b_n, c_n can be explicitly computed in terms of the Fourier coefficients $\hat{f}_n$. Here J_n and Y_n are the Bessel functions of the first and second kinds. The singular values λ_n of the operator $\Lambda_D : L^2(\partial\Omega) \to L^2(\partial D)$ are given by

$$\lambda_n = c_n J_n\left(\frac{\omega}{\sqrt{k}} R'\right) = \frac{A_n J_n(\omega R') - B_n Y_n(\omega R')}{\omega[A_n J_n'(\omega R) - B_n Y_n'(\omega R)]}, \quad n \in \mathbb{Z}, \tag{B.2}$$

where

$$\begin{aligned} A_n &= \frac{1}{\sqrt{k}} Y_n(\omega R') J_n'\left(\frac{\omega}{\sqrt{k}} R'\right) - Y_n'(\omega R') J_n\left(\frac{\omega}{\sqrt{k}} R'\right), \\ B_n &= \frac{1}{\sqrt{k}} J_n(\omega R') J_n'\left(\frac{\omega}{\sqrt{k}} R'\right) - J_n'(\omega R') J_n\left(\frac{\omega}{\sqrt{k}} R'\right). \end{aligned}$$

Since $J_n(x) \sim \frac{1}{(n+1)!}(\frac{x}{2})^n$ and $Y_n(x) \sim \frac{n!}{\pi}(\frac{2}{x})^n$ for $n > 0$, one can see from (B.2) that singular values decay like $(R'/R)^{|n|}$ as the index $|n| \to +\infty$. In short, the singular values of Λ_D decay exponentially.

Appendix C. Generalization to linear elasticity. In this appendix, we extend the approach for the reconstruction of conductivity inclusions to that of elasticity. We restrict ourselves to the two-dimensional case and assume that both $\Omega \setminus \overline{D_*}$ and D_* are occupied by isotropic and homogeneous elastic materials. Let $\mathbf{I}_4$ be the identity 4-tensor and $\mathbf{I}_2$ be the identity 2-tensor (the identity 2×2 matrix). The elastic tensor fields $\mathbb{C}_0$ and $\mathbb{C}_1$ are then of the following form:

$$\mathbb{C}_m = \lambda_m \mathbf{I}_2 \otimes \mathbf{I}_2 + 2\mu_m \mathbf{I}_4, \quad m = 0, 1, \tag{C.1}$$

where (λ_0, μ_0) and (λ_1, μ_1) are the Lamé constants corresponding to $\Omega \setminus \overline{D_*}$ and D_*, respectively, and $(\lambda_0 - \lambda_1)^2 + (\mu_0 - \mu_1)^2 \neq 0$. We also assume that there are two positive constants α_0 and β_0 such that

$$\min(\mu_0, \mu_1) \geq \alpha_0, \quad \min(2\lambda_0 + 2\mu_0, 2\lambda_1 + 2\mu_1) \geq \beta_0, \tag{C.2}$$

which guarantees strong convexity of $\mathbb{C}_0$ and $\mathbb{C}_1$.

Let $\mathbb{C}_{D_*} = \mathbb{C}_0 \chi[\Omega \setminus D_*] + \mathbb{C}_1 \chi[D_*]$ and let $u_*^{(l)}$, $l = 1, \ldots, N$, be the solution to

$$\begin{cases} \nabla \cdot \mathbb{C}_{D_*} \widehat{\nabla} u_*^{(l)} + \omega^2 u_*^{(l)} = 0 & \text{in } \Omega, \\ \dfrac{\partial u_*^{(l)}}{\partial \nu} = g^{(l)} & \text{on } \partial\Omega, \end{cases} \tag{C.3}$$

where $\widehat{\nabla} u_*^{(l)} = \frac{1}{2}(\nabla u_*^{(l)} + (\nabla u_*^{(l)})^t)$ (t for transpose), $\partial u/\partial\nu = (\widehat{\nabla} u)\nu$ denotes here the conormal derivative, and $g^{(l)}, l = 1, \ldots, N$, are given boundary data. The inverse problem here is to reconstruct the elastic inclusion D_* from the boundary measurements $(u_*^{(l)})_{l=1}^N$ on $\partial\Omega$.

As in section 2, a standard approach to solving the inverse problem is to minimize over D the following cost functional:

$$J[D] := \frac{1}{2}\sum_{l=1}^{N}\int_{\partial\Omega}\left|u^{(l)}[D]-u_*^{(l)}\right|^2\,d\sigma, \tag{C.4}$$

where $u^{(l)}[D]$ is the solution to

$$\begin{cases} \nabla\cdot\mathbb{C}_D\widehat{\nabla}u^{(l)}+\omega^2u^{(l)}=0 & \text{in } \Omega,\\ \dfrac{\partial u^{(l)}}{\partial\nu}=g^{(l)} & \text{on } \partial\Omega. \end{cases} \tag{C.5}$$

Here, $\mathbb{C}_D=\mathbb{C}_0\chi[\Omega\setminus D]+\mathbb{C}_1\chi[D]$.

Let

$$p := \frac{\lambda_1(\lambda_0+2\mu_0)}{\lambda_1+2\mu_1} \quad\text{and}\quad q := \frac{4(\mu_1-\mu_0)(\lambda_1+\mu_1)}{\lambda_1+2\mu_1}.$$

Define a 4-tensor $\mathbb{K}$ by

$$\mathbb{K} := p\mathbf{I}_2\otimes\mathbf{I}_2+2\mu_0\mathbf{I}_4+q\mathbf{I}_2\otimes(T\otimes T).$$

Given two 2×2 matrices A and B, we denote $A:B=\sum_{ij}a_{ij}b_{ij}$.

For a given function h on ∂D, the shape derivative of $J[D]$ in the direction of $h\nu$ is given by the same formula as (2.3) but with

$$v^{(l)}[h] := \int_{\partial D} h\mathcal{M}[\widehat{\nabla}u^{(l)}]:\widehat{\nabla}\mathcal{N}^{\omega}[D]\,d\sigma,$$

where

$$\mathcal{M}[\widehat{\nabla}u^{(l)}] := (\mathbb{C}_1-\mathbb{C}_0)\mathbb{C}_1^{-1}\left((\mathbb{K}\widehat{\nabla}u^{(l)}[D]T)\otimes T+(\mathbb{C}_0\widehat{\nabla}u^{(l)}[D]\nu)\otimes\nu\right),$$

and $\mathcal{N}^{\omega}[D]$ is the Green function for $\nabla\cdot\mathbb{C}_D\widehat{\nabla}+\omega^2$ in Ω with homogeneous Neumann boundary conditions corresponding to $\delta_y I_2$. See [15, 3].

To explicitly compute the shape derivative of J, we again introduce the adjoint state $p^{(l)}[D]$ as the solution to

$$\begin{cases} \nabla\cdot\mathbb{C}_D\widehat{\nabla}p^{(l)}[D]+\omega^2p^{(l)}[D]=0 & \text{in } \Omega,\\ \dfrac{\partial p^{(l)}[D]}{\partial\nu}=(u^{(l)}[D]-u_*^{(l)}) & \text{on } \partial\Omega, \end{cases} \tag{C.6}$$

which is given in the elastic case by

$$p^{(l)}[D](x)=\int_{\partial\Omega}(u^{(l)}[D]-u_*^{(l)})(y)\mathcal{N}^{\omega}[D](x,y)\,d\sigma(y).$$

Using $p^{(l)}$ to express the integral

$$\int_{\partial\Omega}(u^{(l)}[D]-u_*^{(l)})\overline{v^{(l)}[h]}\,d\sigma,$$

we arrive at

$$(d_{\mathcal{S}}J[D], h) = \int_{\partial D} h\, \Re e \sum_{l=1}^{N} \left(\mathcal{M}[\widehat{\nabla} u^{(l)}] : \widehat{\nabla} p^{(l)}[D] \right) d\sigma. \tag{C.7}$$

Set

$$w_n = \Re e \sum_{l=1}^{N} \left(\mathcal{M}[\widehat{\nabla} u^{(l)}[D_{n-1}]] : \widehat{\nabla} p^{(l)}[D_{n-1}] \right).$$

A first algorithm then consists of replacing, at each step n,

$$\partial D_{n-1} \mapsto \partial D_n := \partial D_{n-1} + h_n \nu,$$

where

$$h_n - J[D_{n-1}] \frac{w_n}{\int_{\partial D} w_n^2 \, d\sigma}. \tag{C.8}$$

On the other hand, if we define $\{f_i[D] \,:\, i = 1, \ldots, M\}$ as the significant singular vectors associated with the operator $\Lambda_D : L^2(\partial\Omega) \to L^2(\partial D)$ given by

$$\Lambda_D(f) = p|_{\partial D},$$

with

$$\begin{cases} \nabla \cdot \mathbb{C}_D \widehat{\nabla} p + \omega^2 p = 0 & \text{in } \Omega, \\ \dfrac{\partial p}{\partial \nu} = f & \text{on } \partial\Omega, \end{cases}$$

then in our new approach the update h_n is chosen as in (3.14), with

$$w_i^{(l)}[D_{n-1}] = \mathcal{M}[\widehat{\nabla} u^{(l)}[D_{n-1}]] : \widehat{\nabla} p_i[D_{n-1}],$$

$$p_i[D_{n-1}] = \Lambda_{D_{n-1}}[f_i[D_{n-1}]],$$

and

$$\alpha_{il}[D_{n-1}] := \int_{\partial\Omega} (u^{(l)}[D_{n-1}] - u_*^{(l)}) \cdot \overline{f_i}[D_{n-1}] \, d\sigma, \quad i = 1, \ldots, M, \ l = 1, \ldots, N.$$

Acknowledgments. The authors are very grateful to the reviewers for their comments and suggestions which improved the presentation of the paper.

REFERENCES

[1] H. Ammari, *An Introduction to Mathematics of Emerging Biomedical Imaging*, Math. Appl. 62, Springer-Verlag, Berlin, 2008.

[2] H. Ammari, E. Beretta, E. Francini, H. Kang, and M. Lim, *Optimization algorithm for reconstructing interface changes of a conductivity inclusion from modal measurements*, Math. Comp., 79 (2010), pp. 1757–1777.

[3] H. Ammari, E. Beretta, E. Francini, H. Kang, and M. Lim, *Reconstruction of small interface changes of an inclusion from modal measurements* II: *The elastic case*, J. Math. Pures Appl., 94 (2010), pp. 322–339.

[4] H. Ammari, J. Garnier, H. Kang, M. Lim, and K. Sølna, *Multistatic imaging of extended targets*, SIAM J. Imaging Sci., 5 (2012), pp. 564–600.

[5] H. Ammari, J. Garnier, and K. Sølna, *Resolution and stability analysis in full-aperture, linearized conductivity and wave imaging*, Proc. Amer. Math. Soc., to appear.

[6] H. Ammari, E. Iakovleva, and D. Lesselier, *Two numerical methods for recovering small inclusions from the scattering amplitude at a fixed frequency*, SIAM J. Sci. Comput., 27 (2005), pp. 130–158.

[7] H. Ammari and H. Kang, *Reconstruction of Small Inhomogeneities from Boundary Measurements*, Lecture Notes in Math. 1846, Springer, Berlin, 2004.

[8] H. Ammari and H. Kang, *Expansion methods*, in Handbook of Mathematical Methods in Imaging, Springer, New York, 2011, pp. 447–499.

[9] H. Ammari, H. Kang, E. Kim, K. Louati, and M. Vogelius, *A MUSIC-type algorithm for detecting internal corrosion from electrostatic boundary measurements*, Numer. Math., 108 (2008), pp. 501–528.

[10] H. Ammari, H. Kang, and H. Lee, *Layer Potential Techniques in Spectral Analysis*, Math. Surveys Monogr. 153, Amer. Math. Soc., Providence, 2009.

[11] H. Ammari, H. Kang, H. Lee, and W.-K. Park, *Asymptotic imaging of perfectly conducting cracks*, SIAM J. Sci. Comput., 32 (2010), pp. 894–922.

[12] H. Ammari, H. Kang, M. Lim, and H. Zribi, *Conductivity interface problems. Part* I: *Small perturbations of an interface*, Trans. Amer. Math. Soc., 362 (2010), pp. 2435–2449.

[13] G. Bao, S. Hou, and P. Li, *Recent studies on inverse medium scattering problems*, in Modelling and Computations in Electromagnetics, Lecture Notes in Comput. Sci. Eng. 59, Springer, Berlin, 2008, pp. 165–186.

[14] E. Beretta and E. Francini, *Asymptotic formulas for perturbations in the electromagnetic fields due to the presence of thin inhomogeneities*, in Inverse Problems: Theory and Applications, Contemp. Math. 333, Amer. Math. Soc., Providence, RI, 2003, pp. 49–62.

[15] E. Beretta and E. Francini, *An asymptotic formula for the displacement field in the presence of thin elastic inhomogeneities*, SIAM J. Math. Anal., 38 (2006), pp. 1249–1261.

[16] M. Burger and S. J. Osher, *A survey on level set methods for inverse problems and optimal design*, European J. Appl. Math., 16 (2005), pp. 263–301.

[17] T. F. Chan and X.-C. Tai, *Identification of discontinuous coefficients in elliptic problems using total variation regularization*, SIAM J. Sci. Comput., 25 (2003), pp. 881–904.

[18] T. F. Chan and X. C. Tai, *Level set and total variation regularization for elliptic inverse problems with discontinuous coefficients*, J. Comput. Phys., 193 (2004), pp. 40–66.

[19] S. Chen, B. Merriman, S. Osher, and P. Smereka, *A simple level set method for solving Stefan problems*, J. Comput. Phys., 135 (1997), pp. 8–29.

[20] Z. Chen and J. Zou, *An augmented Lagrangian method for identifying discontinuous parameters in elliptic systems*, SIAM J. Control Optim., 37 (1999), pp. 892–910.

[21] M. Cheney, *The linear sampling method and the MUSIC algorithm*, Inverse Problems, 17 (2001), pp. 591–595.

[22] E. DiBenedetto, C. M. Elliott, and A. Friedman, *The free boundary of a flow in a porous body heated from its boundary*, Nonlinear Anal. Theory Meth. Appl., 10 (1986), pp. 879–900.

[23] S. Hou, K. Solna, and H. Zhao, *Imaging of location and geometry for extended targets using the response matrix*, J. Comput. Phys., 199 (2004), pp. 317–338.

[24] V. Isakov, *On uniqueness of recovery of a discontinuous conductivity coefficient*, Comm. Pure Appl. Math., 41 (1988), pp. 865–877.

[25] K. Ito, B. Jin, and J. Zou, *A direct sampling method to an inverse medium scattering problem*, Inverse Problems, 28 (2012), 025003.

[26] K. Ito, K. Kunish, and Z. Li, *Level-set function approach to an inverse interface problem*, Inverse Problems, 17 (2001), pp. 1225–1242.

[27] K. Ito, K. Kunisch, and G. H. Peichl, *Variational approach to shape derivatives*, ESAIM Control Optim. Calc. Var., 14 (2008), pp. 517–539.

[28] B. Jadamba, A. A. Khan, and F. Raciti, *On the inverse problem of identifying Lamé coefficients in linear elasticity*, Comput. Math. Appl., 56 (2008), pp. 431–443.

[29] A. Kirsch and N. Grinberg, *The Factorization Method for Inverse Problems*, Oxford Lecture Ser. Math. Appl. 36, Oxford University Press, Oxford, UK, 2008.

[30] D. R. Luke and A. J. Devaney, *Identifying scattering obstacles by the construction of non-scattering waves*, SIAM J. Appl. Math., 68 (2007), pp. 271–291.

[31] S. Mallat, *A Wavelet Tour of Signal Processing*, Academic Press, San Diego, 1998.

[32] P. Maponi, L. Misici, and F. Zirilli, *Three-dimensional time harmonic inverse electromagnetic scattering*, in Inverse Problems in Mathematical Physics, Lecture Notes in Phys. 422, Springer, Berlin, 1993, pp. 139–147.

[33] L. Misici and F. Zirilli, *Three-dimensional inverse obstacle scattering for time harmonic acoustic waves: A numerical method*, SIAM J. Sci. Comput., 15 (1994), pp. 1174–1189.

[34] C. Prada and M. Fink, *Eigenmodes of the time-reversal operator: A solution to selective focusing in multiple-target media*, Wave Motion, 20 (1994), pp. 151–163.

[35] M. Raessi, J. Mostaghimi, and M. Bussmann, *Advecting normal vectors: A new method for calculating interface normals and curvatures when modeling two-phase flows*, J. Comput. Phys., 226 (2007), pp. 774–797.

[36] F. Santosa, *A level-set approach for inverse problems involving obstacles*, ESAIM Contol Optim. Calc. Var., 1 (1995/1996), pp. 17–33.

[37] C. F. Tolmasky and A. Wiegmann, *Recovery of small perturbations of an interface for an elliptic inverse problem via linearization*, Inverse Problems, 15 (1999), pp. 465–487.

[38] J. Xie and J. Zou, *Numerical reconstruction of heat fluxes*, SIAM J. Numer. Anal., 43 (2005), pp. 1504–1535.